Available online at www.sciencedirect.com

ScienceDirect

IFAC Papers Online CONFERENCE PAPER ARCHIVE

IFAC PapersOnLine 51-29 (2018) 348–353

Input-Constrained Path Following for Autonomous Marine Vehicles with a Global Region of Attraction ⋆

Nguyen T. Hung * **F. Rego** *,** **N. Crasta** * **A. M. Pascoal** *

* *Laboratory of Robotics and Systems in Engineering and Science(LARSyS), ISR/IST, University of Lisbon, Lisbon, Portugal* {*hungnguyen,frego,ncrasta,antonio*}*@isr.ist.utl.pt.*

** *Automatic Control Laboratory, EPFL, Switzerland*

Abstract: This paper presents a solution to the problem of path following control for autonomous marine vehicles (AMVs) subject to input constraints and constant ocean current disturbances. We propose two nonlinear control strategies: the first is obtained by using a Lyapunov-based design method, while the second is developed by adopting a Model Predictive Control (MPC) framework. We show that, with the proposed control strategies, the path-following error is globally asymptotically stable (GAS). Simulations with a kinematic model of the vehicle support the theoretical results. Simulations with a realistic model of the Medusa class of AMVs show the robustness of the proposed control strategies.

Keywords: AMVs, Path following, MPC, Input constraint.

1. INTRODUCTION

Along with point stabilization and trajectory tracking, path following is one of the fundamental motion control problems of autonomous marine vehicles, which are normally under-actuated, see (De Luca et al. (1998)) for an overview of these problems. Path following is useful in a number of practical applications that include, for example, mapping of underwater habitats, where the key objective is to obtain a map of a given area without overly restrictive temporal specifications. From a technical standpoint, when compared to trajectory tracking, path following has the potential to exhibit smoother convergence properties and reduced actuator activity (Aguiar and Hespanha (2007); De Luca et al. (1998)).

The last two decades have witnessed a considerable interest in the path following problem because of its wide range of practical applications and theoretical challenges. By formulating the path following problem as a stabilization problem in a conveniently defined path following error space, a large number of methods have been proposed to asymptotically stabilize the path following error system about the origin; see for example (Caharija et al. (2016); Lapierre et al. (2006)) and the references therein. In this context, Lyapunov-based techniques - that target explicitly the design of stabilizing control laws for nonlinear systems - have become a popular tool to solve several variants of the path following problem. However, many of the results published on the use of Lyapunov-based design techniques do not take input constraints directly into account. As a consequence, proper care must be taken to ensure that the resulting systems end up operating in a small region where the control law for the unconstrained system does not violate the constraints.

In recent years, thanks to its ability to handle input and even state constrains explicitly, Model Predictive Control has become the method par excellence to solve more challenging versions of the path following problem, see for instance (Alessandretti et al. (2013); Yu et al. (2015)). In this set-up, a stabilizing MPC for a path following error system is designed with a terminal cost and a terminal set so as to guarantee *recursive feasibility and stability* of the MPC scheme. In (Yu et al. (2015)), the terminal set is designed locally using a polytopic linear differential inclusion method. The approach reported in (Alessandretti et al. (2013)) aims to enlarge the terminal set by resorting to the stabilizing nonlinear path following control law proposed in (Aguiar and Hespanha (2007)). The main drawback of these two approaches is the presence of the terminal set, which implies that the region of attraction is local. Furthermore, it is very difficult to characterize the region of attraction to determine the region where the vehicle should start.

Motivated by these considerations, in this paper we propose two control strategies for the path following problem of AMVs subject to input constraints and disturbances caused by constant ocean currents. The main contribution of the paper lies in the fact that the proposed control strategies are not only able to handle the input constraints of the vehicle explicitly but also yield a global region of attraction, meaning that regardless of any initial position and orientation, it is always guaranteed the vehicle converges to the path asymptotically. In addition, in contrast with the assumptions in (Alessandretti et al. (2013)), the vehicle's speed is constrained to be non-negative. This is extremely important not only for certain types of marine vehicles but also for fixed wing UAVs. Finally, constant

⋆ This research was supported in part by the Marine UAS project under the Marie Curie Sklodowska grant agreement No 642153, the H2020 EU Marine Robotics Research Infrastructure Network (Project ID 731103), and the FCT Project UID/EEA/5009/2013.

10.1016/j.ifacol.2018.09.499

ocean currents are also taken explicitly into account.
The paper is organized as follow. Section 2 presents the formulation of the input-constrained path following problem. Section 3 describes the design and theoretical results of the proposed path following control strategies. Simulations are presented in Section 4. Finally, Section 5 contains the main conclusions.

2. INPUT-CONSTRAINED PATH FOLLOWING

In what follows, $\{\mathcal{I}\} = \{x_\mathcal{I}, y_\mathcal{I}, z_\mathcal{I}\}$ and $\{\mathcal{B}\} = \{x_\mathcal{B}, y_\mathcal{B}, z_\mathcal{B}\}$ denote an inertial North-East-Down (NED) frame and a body-fixed frame, respectively. In the marine literature, see Fossen (2011), the axis $x_\mathcal{I}$ normally points to the North, the axis $y_\mathcal{I}$ points to the East, and the axis $z_\mathcal{I}$ points downward, normal to the Earth's surface, . Let P be the center of mass of the vehicle and denote by $\mathbf{p} = [x, y, z]^{\mathrm{T}} \in \mathbb{R}^3$ the position of P in $\{\mathcal{I}\}$. For simplicity of exposition, we assume that the vehicle moves in a horizontal plane; without loss of generality, we make $z = 0$. Let $\mathcal{P}$ be a planar path that the vehicle must follow, parameterized by its arc length s.
We assume the motion of the vehicle is disturbed by a constant ocean current represented by a vector $\mathbf{v}_c = [v_{\mathrm{cx}}, v_{\mathrm{cy}}]^{\mathrm{T}} \in \mathbb{R}^2$ expressed in the inertial frame $\{\mathcal{I}\}$. The 3-DOF kinematic model of the vehicle is described by

$$\begin{aligned} \dot{x} &= u_{\mathrm{r}} \cos\psi - v_{\mathrm{r}} \sin\psi + v_{\mathrm{cx}}, \\ \dot{y} &= u_{\mathrm{r}} \sin\psi + v_{\mathrm{r}} \cos\psi + v_{\mathrm{cy}}, \\ \dot{\psi} &= r, \end{aligned} \tag{1}$$

where $u_{\mathrm{r}}, v_{\mathrm{r}}$ denote the surge and sway speed components, respectively, of the velocity vector $\mathbf{v}_{\mathrm{b}} = [u_{\mathrm{r}}, v_{\mathrm{r}}]^{\mathrm{T}}$ of the vehicle with respect to the fluid, expressed in the body frame, ψ is the yaw angle, and r is the yaw rate. For a large class of under-actuated AMVs such as Medusa and Delfim(Abreu et al. (2016), or Charlie (Bibuli et al. (2009)) the sway speed is in practice so small that it can be neglected. For this reason, in this work we consider $v_{\mathrm{r}} = 0$ and therefore $\mathbf{v}_{\mathrm{b}} = [u_{\mathrm{r}}, 0]^{\mathrm{T}}$. We denote by $\mathbf{v} = [\dot{x}, \dot{y}]^{\mathrm{T}}$ the total velocity vector of the vehicle in the inertial frame $\{\mathcal{I}\}$ and its magnitude (inertial speed of the vehicle) by $U := \|\mathbf{v}\|$. We also denote by χ the course angle, defined by the orientation of the total velocity vector in the inertial frame, defined as $\chi = \arctan 2(\dot{y}, \dot{x})$. With this notation, the kinematics of the AMV can be rewritten as

$$\dot{x} = U\cos(\chi), \quad \dot{y} = U\sin(\chi) \tag{2a}$$

$$\dot{\chi} = r_\chi = r\left(1 - \frac{\|\mathbf{v_c}\|\cos(\alpha-\psi)}{m}\right) - \frac{\dot{U}\|\mathbf{v_c}\|\sin(\alpha-\psi)}{Um}, \tag{2b}$$

where r_χ denotes the course rate, $\alpha = \arctan 2(v_{\mathrm{cy}}, v_{\mathrm{cx}})$, and $m = \sqrt{U^2 - \|\mathbf{v_c}\|^2 \sin^2(\alpha-\psi)}$ (see the Appendix for details). Notice that, without ocean current, (2) resembles those of a unicycle model (Lapierre et al. (2006)) with input vector (u_{r}, r). Notice also that when $\|\mathbf{v_c}\| = 0$, that is, in the absence of ocean currents, r_χ=r. We assume that the total speed U and the course rate r_χ can be tracked by an autopilot that admits input commands in the set

$$\mathbb{U}_v := \{(U, r_\chi) : 0 \le U \le U_{\max}, |r_\chi| \le r_{\chi\max}\}, \tag{3}$$

where $U_{\max}, r_{\chi\max}$ are saturation values. Notice that, in practice, it is common that the autopilot admits the heading rate rather than the course rate. Given $r_{\max}$ (a constraint on the heading rate such that $|r| \le r_{\max}$), $\|\mathbf{v_c}\|_{\max}$ (an upper bound on the magnitude of the ocean current), and $U_{\min}$ (a lower bound of the total inertial speed of the vehicle), $r_{\chi\max}$ can be easily computed from (2b) such that for any angle $(\alpha - \psi)$, if the computed course rate lies in the constraint set, then the heading rate computed from the course rate and (2b) satisfies the heading rate constraint. Obviously, without ocean current the course angle coincides with the heading, and therefore $r_{\chi\max} = r_{\max}$.
Referring to the Fig. 2.1, let S be an arbitrary point on the path and let s be the signed curvilinear abscissa of S along the path which, we recall that, is parameterized by its arc length. Attached to S, consider a parallel transport frame $\{\mathcal{F}\} = \{x_\mathcal{F}, y_\mathcal{F}, z_\mathcal{F}\}$ with the origin at S and its axis defined as follows: $x_\mathcal{F}$ is aligned with the tangent to the path at S and points in the direction of increasing path length, $z_\mathcal{F}$ points downward to the Earth's surface, and $y_\mathcal{F}$ is determined by the positive right-hand rule. In the set-up adopted for path-following, the *parallel transport frame* moves along the path in a manner to be determined and plays the role of a virtual "reference" for position and course angle that the vehicle must track to achieve good path following. This yields an extra degree of freedom that allows us to use the linear speed $\dot{s}$ of the virtual "reference" along the path as a control input to aid in the solution of the path following problem. See (Lapierre et al. (2006)) and the references therein for an introduction to this methodology.
As illustrated in Fig. 2.1, given an arbitrary point S on

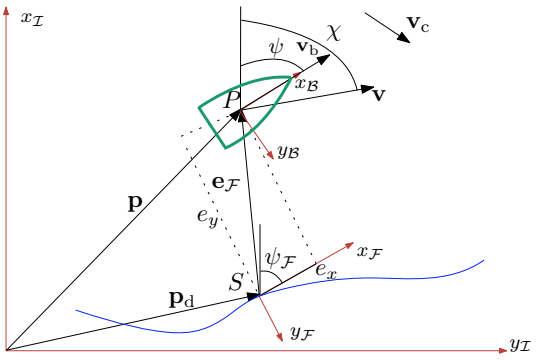

Fig. 2.1. Vehicle position expressed in the reference frame. $\mathbf{v}_c$ is the ocean current. The sway velocity is neglected, i.e. $v_{\mathrm{r}} = 0$.

the path we let $\mathbf{e}_\mathcal{F} = [e_x, e_y, 0]^T$ be the position vector of the vehicle expressed in the *parallel transport frame* at S, that is, the position error between the vehicle and the path. Let $\kappa(s)$ and $\psi_\mathcal{F}$ be the curvature of the path and the angle that the tangent to the path makes with $x_\mathcal{I}$, respectively, at S. Clearly, the orientation error between the vehicle and the *parallel transport frame* is given by $\psi_e = \chi - \psi_\mathcal{F}$. Let $v = \dot{s}$ be the speed of the virtual "reference", $\mathbf{x} = [e_x, e_y, \psi_e]^{\mathrm{T}}$ the path following error vector containing the position and orientation errors and $\mathbf{u} = [U, v, r_\chi]^{\mathrm{T}}$ the input vector. Using the methodology exposed in Lapierre et al. (2006) for wheeled robots, straightforward computations show that the evolution of the path following error vector is described by the dynamic equation

$$\dot{\mathbf{x}} = \mathbf{f}(\mathbf{x}, \mathbf{u}) = \begin{bmatrix} -v(1-\kappa(s)e_y) + U\cos(\psi_e) \\ -\kappa(s)e_x v + U\sin(\psi_e) \\ r_\chi - \kappa(s)v \end{bmatrix}. \quad (4)$$

Later, as we shall see, for design purposes, we impose a constraint on v, that is, $|v| \leq v_{\max}$, where $v_{\max}$ is a parameter that will be specified later.

We are now in a position to formulate the following input-constrained path following problem.

The Input-Constrained Path Following Problem. *Given a spatial path $\mathcal{P}$ parameterized by its arc length s, a positive desired speed profile $v_{\mathrm{d}}(s)$ along the path, and the input constraint set $\mathbb{U}_v$ defined by* (3)*, derive a feedback control law for $(U, r_\chi) \in \mathbb{U}_v$ and v, with $|v| \leq v_{\max}$ so as to drive the path following error dynamics described in* (4) *asymptotically to zero, while ensuring also asymptotically that v tracks the desired speed profile $v_{\mathrm{d}}(s)$, that is, $v(t) - v_{\mathrm{d}}(s(t))$ tends to zero.*

3. MAIN RESULTS

In this section, two input-constrained nonlinear controllers are proposed to solve the constrained path following problem. The first controller is developed by resorting to a Lyapunov-based method, whereas the second is derived using MPC.

3.1 Input-Constrained Path Following with a Lyapunov Based Controller

In what follows we require that the input constraints, the path specifications, and the ocean current satisfy the following assumptions.

Assumption 1.

- A1.1 The vehicle inner loops guarantee that the references for U and r (and therefore r_χ) can be tracked accurately. Thus, we neglect the dynamics of the inner loops.
- A1.2 The desired speed profile is assigned so that $\max(v_{\mathrm{d}}(s)) \leq U_{\max}$ and $\min(v_{\mathrm{d}}(s)) > \|\mathbf{v_c}\|_{\max}$.
- A1.3 The constraint imposed for the speed of the virtual reference, $v_{\max}$, satisfies $v_{\max} > \max(v_{\mathrm{d}}(s))$.
- A1.4 The curvature of the path is sufficiently smooth and bounded such that the angular rate of the path satisfies $\max(\kappa(s))v_{\max} < r_{\chi\max}$.
- A1.5 The ocean current can be either measured or estimated.

Remark 1. Assumption A1.2 implies that if the current is strong, the desired speed profile should be large enough so as to make the vehicle move forward. In addition, it also implies that the surge speed u_{r} is always positive, thus forcing the vehicle to always move forward with respect to the water. Assumptions A1.3 and A1.4 are included to ensure that the vehicle and the virtual reference can "catch up with each other". Assumption A1.5 allows us to compute the heading rate r from r_χ. In practice, because it is difficult to measure the ocean current, one can estimate it using the kinematic model of the vehicle given by (1)*, see the current estimator in (Vanni et al. (2008)).*

We next show that there exists a global nonlinear control law that satisfies the input constraints and stabilizes the path following error dynamics described by (4).

Theorem 1. (Lyapunov-based controller) *Consider the path following error system* (4) *subjected to the vehicle input constraint given by* (3) *and $|v| \leq v_{\max}$. Further, let Assumption 1 hold true. Then, the Lyapunov-based control law given by*

$$\mathbf{u}_{\mathrm{L}}(\mathbf{x}) = \begin{bmatrix} U \\ v \\ r_\chi \end{bmatrix} = \begin{bmatrix} v_{\mathrm{d}}(s) \\ U\cos(\psi_e) + k_1\tanh(e_x) \\ -\frac{ke_yU\sin(\psi_e)}{(1+e_x^2+e_y^2)\psi_e} - k_2\tanh(\psi_e) + \kappa(s)v \end{bmatrix} \quad (5)$$

solves the input constrained-path following problem, where $k_1, k_2, k \in \mathbb{R}_{>0}$ are tuning parameters that satisfy

$$\begin{aligned} 0 < k_1 &\leq v_{\max} - \max(v_{\mathrm{d}}(s)), \\ 0.5k\max(v_{\mathrm{d}}(s)) + k_2 &\leq r_{\chi\max} - \max(\kappa(s))v_{\max}. \end{aligned} \quad (6)$$

Furthermore, the control law given by (5) *renders the origin of* (4) *globally asymptotically stable.*

PROOF: *Feasibility.* Since $v_{\mathrm{d}}(s) > 0$ and Assumption A1.2 holds, U trivially satisfies (3). From (5), it follows immediately that

$$|v| = |v_{\mathrm{d}}(s)\cos\psi_e + k_1\tanh(e_x)| \leq v_{\mathrm{d}}(s) + k_1.$$

Now Assumption A1.3 implies that $(v_{\max} - \max(v_{\mathrm{d}}(s)) > 0$. Let $k_1 > 0$ be such that (6) satisfied. Then, clearly $|v| \leq v_{\max}$. As for the constraint on the course rate, we note the inequality $|e_y/(1+e_x^2+e_y^2)| \leq 1/2$ and the fact that $\sin(\psi_e)/\psi_e \leq 1$ holds for all e_x, e_y, ψ_e. Using these facts, we have

$$\begin{aligned} |r_\chi| &= \left| -\frac{ke_yU\sin\psi_e}{(1+e_x^2+e_y^2)\psi_e} - k_2\tanh(\psi_e) + \kappa(s)v \right| \\ &\leq 0.5k\max(v_{\mathrm{d}}(s)) + k_2 + \max(\kappa(s))v_{\max}. \end{aligned}$$

Thus, by proper selection of the positive constants k, k_2 satisfying (6), we can conclude that $r_\chi \leq r_{\chi\max}$.

Global Asymptotic Stability. We consider the Lyapunov function candidate given by

$$V_{\mathrm{L}}(\mathbf{x}) = \frac{k}{2}\log(1+e_x^2+e_y^2) + \frac{1}{2}\psi_e^2 \quad (7)$$

with $k > 0$ as given above. Computing the derivative of the Lyapunov function and replacing the inputs by the control law (5) yields

$$\dot{V}_{\mathrm{L}} = -\frac{kk_1e_x\tanh(e_x)}{1+e_x^2+e_y^2} - k_2\psi_e\tanh(\psi_e) \leq 0, \ \forall \mathbf{x}.$$

Observe that $\dot{V}_{\mathrm{L}} = 0$ when $e_x = 0$ and $\psi_e = 0$. We now consider the set $\Omega := \{\mathbf{x} \in \mathbb{R}^3 | e_x = 0, \psi_e = 0\}$. In Ω, since $\lim_{\psi_e \to 0} \sin\psi_e/\psi_e = 1$, replacing the input $\mathbf{u}$ in (4) by (5), we obtain $\dot{\psi}_e = -ke_yU/(1+e_y^2)$. It is clear that, in Ω, if $\psi_e(t) \equiv 0$ then it follows that $\dot{\psi}_e(t) \equiv 0$, and as a consequence $e_y(t) \equiv 0$. Further, since V_{L} is radially unbounded, invoking corollary 4.2 of LaSalle's theorem (Khalil (2002)), we conclude that the origin of the path following error system is GAS. □

3.2 Input-Constrained Path Following with MPC

The Lyapunov-based controller in the previous subsection solves the input-constrained path following problem. However, the convergence of the path following error to origin can be slow (as can be seen from the derivative of the Lyapunov function in the proof of *Theorem 1*, the convergence rate is slow when e_x, ψ_e are small, regardless of e_y). In

this subsection, we adopt a sampled-data MPC framework which is also referred as Lyapunov-based MPC (see de la Pena and Christofides (2008)) to solve the constrained path following problem and speed up the convergence rate. To this end, we employ the Lyapunov function (7) and the Lyapunov-based controller (5) to construct a contractive constraint that forces the decrease rate of the Lyapunov function with the MPC controller to be faster than with the Lyapunov-based controller. In addition, by inheriting the feasibility and stability with the control law (5), it follows that terminal constraint and terminal cost, two ingredients in the general stabilizing MPC framework (see Mayne et al. (2000)), are no longer necessary.

First, we assign the speed of the vehicle as the desired speed profile, that is, $U = v_{\rm d}(s)$. The dynamics of the path following error system (4) can be rewritten as

$$\dot{\mathbf{x}} = \mathbf{f}(\mathbf{x}, \mathbf{u}) = \begin{bmatrix} -v(1-\kappa(s)e_y) + v_{\rm d}(s)\cos(\psi_e) \\ -\kappa(s)e_x v + v_{\rm d}(s)\sin(\psi_e) \\ r_\chi - \kappa(s)v \end{bmatrix}, \quad (8)$$

where $\mathbf{u} = [v, r_\chi]^{\rm T}$ is the input vector that is constrained in a set $\mathbb{U}$ given by

$$\mathbb{U} := \{(v, r_\chi) : |v| \le v_{\max}, |r_\chi| \le r_{\chi\max}\}. \quad (9)$$

We define a finite horizon open loop optimal control problem (FOCP), denoted $\mathcal{OCP}(t, \mathbf{x}(t), s(t), T_{\rm p})$, where $T_{\rm p}$ is the prediction horizon that the sampled data MPC solves at every sampling time as follows:

Definition 1. $\mathcal{OCP}(t, \mathbf{x}(t), s(t), T_{\rm p})$

$$\min_{\bar{\mathbf{u}}(\cdot)} J_{T_{\rm p}}(\mathbf{x}(t), s(t), \bar{\mathbf{u}}(\cdot)) \quad (10)$$

with

$$J_{T_{\rm p}}(\mathbf{x}(t), s(t), \bar{\mathbf{u}}(\cdot)) := \int_t^{t+T_{\rm p}} l(\bar{\mathbf{x}}(\tau), \bar{s}(\tau), \bar{\mathbf{u}}(\tau))\, {\rm d}\tau$$

subject to

$$\dot{\bar{\mathbf{x}}}(\tau) = \mathbf{f}(\bar{\mathbf{x}}(\tau), \bar{\mathbf{u}}(\tau)), \tau \in [t, t+T_{\rm p}], \bar{\mathbf{x}}(t) = \mathbf{x}(t), \quad (11a)$$

$$\dot{\bar{s}}(\tau) = v(\tau), \quad \tau \in [t, t+T_{\rm p}], \quad \bar{s}(t) = s(t), \quad (11b)$$

$$\bar{\mathbf{u}}(\tau) \in \mathbb{U}, \quad \tau \in [t, t+T_p], \quad (11c)$$

$$\frac{\partial V}{\partial \mathbf{x}}\mathbf{f}(\mathbf{x}(t), \bar{\mathbf{u}}(t)) \le \frac{\partial V}{\partial \mathbf{x}}\mathbf{f}(\mathbf{x}(t), \mathbf{u}_{\rm n}(\mathbf{x}(t))). \quad (11d)$$

In (11), we use the bar notation to denote the predicted variables and to differentiate from the actual variables which do not have a bar. Specifically, $\bar{\mathbf{x}}(\tau)$ is the predicted trajectory of the path following error and $\bar{s}(\tau)$ is the predicted value of the path parameter s. Both are computed using the dynamic model (8) and the initial conditions (11a) and (11b), driven by the input $\bar{\mathbf{u}}(\tau)$ with $\tau \in [t, t+T_{\rm p}]$ over the prediction horizon $T_{\rm p}$. We stress that in the MPC scheme above, we do not require a terminal set and a terminal cost, which are normally designed to ensure recursive feasibility and stability. Instead, we add the constraint (11d) which is referred as a *contractive constraint* to guarantee stability. This constraint is constructed based on a global Lyapunov function $V : \mathbb{R}^3 \to \mathbb{R}_{\ge 0}$ and its associated stabilizing constrained control law $\mathbf{u}_{\rm n} : \mathbb{R}^3 \to \mathbb{U}$. Finally, $l : \mathbb{R}^3 \times \mathbb{U} \times \mathbb{R} \to \mathbb{R}_{\ge 0}$ is the stage cost of the objective functional $J_{T_{\rm p}}$.

In the sampled data MPC scheme, the optimal control problem $\mathcal{OCP}(t, \mathbf{x}(t), s(t), T_{\rm p})$ is repeatedly solved at every discrete sampling instant $t_i = i\delta$, $i \in \mathbb{N}_+$, where δ is a sampling interval. Let $\bar{\mathbf{u}}^*(\tau), \tau \in [t, t+T_{\rm p}]$, be the optimal solution of the optimal control problem $\mathcal{OCP}(t, \mathbf{x}(t), s(t), T_{\rm p})$. Then, the MPC control law $\mathbf{u}_{\rm mpc}(\cdot)$ is then defined as

$$\mathbf{u}_{\rm mpc}(t) = \bar{\mathbf{u}}^*(t), \ t \in [t_i, t_i + \delta]. \quad (12)$$

Before proceeding to the main result for the path following problem with the proposed MPC scheme, we make the following assumptions.

Assumption 2.

A2.1 The stage cost $l(\cdot)$ is continuous and $l(\cdot) = 0$ when $\mathbf{x} = \mathbf{0}$ and $\mathbf{u}_{\rm a} = [-v + v_{\rm d}(s)\cos\psi_e, r_\chi - \kappa(s)v]^{\rm T} = \mathbf{0}$.

A2.2 Given the path following error dynamics in (8), there exists a global Lyapunov function $V : \mathbb{R}^3 \to \mathbb{R}_{\ge 0}$ such that V is positive definite and $V(\mathbf{x}) = 0$ if and only if $\mathbf{x} = \mathbf{0}$ and an associated nonlinear feedback control law $\mathbf{u}_{\rm n} : \mathbb{R}^3 \to \mathbb{U}$ that satisfies $\frac{\partial V}{\partial \mathbf{x}}\mathbf{f}(\mathbf{x}, \mathbf{u}_{\rm n}(\mathbf{x})) \le 0$ for all $\mathbf{x} \ne \mathbf{0}$. Furthermore, $\mathbf{u}_{\rm n}(\mathbf{x})$ globally stabilizes (8).

Remark 2. Assumption A2.1 *is motivated by the fact that* $\mathbf{u}_{\rm a} \to \mathbf{0}$ *once the path following error is stabilized.*

We are in the position to state the main result of this subsection.

Theorem 2. MPC for Path Following (MPC-PF).
Consider the path following error system (8) *and let Assumption 2 holds true. Then, with a sufficiently small sampling interval* δ*, the proposed sampled data MPC scheme solves the constrained path following problem. Furthermore, the origin of the resulting path following error system is GAS.*

PROOF: *Recursive feasibility.* Since $l(\cdot)$ is continuous and defined over the compact set $\mathbb{U}$, the optimal control problem $\mathcal{OCP}(t, \mathbf{x}(t), s(t), T_{\rm p})$ is always feasible. Clearly, $\bar{\mathbf{u}}(\tau) = \mathbf{u}_{\rm n}(\mathbf{x}(t)), \tau \in [t, t+\delta]$ is one of the feasible solutions for $\bar{\mathbf{u}}(\tau)$ for $\tau \in [t, t+\delta]$ satisfying constraints (11c) and (11d), while the rest of $\bar{\mathbf{u}}(\tau), \tau \in [t+\delta, t+T_{\rm p}]$ can be chosen freely in the input space $\mathbb{U}$ since there are no other constraints imposed on it.

Global asymptotic stability. Consider the Lyapunov function V that satisfies *Assumption A2.2* for the path following error system (8) controlled by the proposed MPC scheme. The *contractive constraint* (11d) and *Assumption A2.2* imply that

$$\dot{V}(t) = \frac{\partial V}{\partial \mathbf{x}}\mathbf{f}(\mathbf{x}(t), \mathbf{u}_{\rm mpc}(t)) \le \frac{\partial V}{\partial \mathbf{x}}\mathbf{f}(\mathbf{x}(t), \mathbf{u}_{\rm n}(\mathbf{x}(t))) \le 0.$$

We consider two cases of $\mathbf{u}_{\rm mpc}(t)$. In the first case, $\mathbf{u}_{\rm mpc}(t) \ne \mathbf{u}_{\rm n}(\mathbf{x}(t))$ that results in $\dot{V}(t) = \frac{\partial V}{\partial \mathbf{x}}\mathbf{f}(\mathbf{x}(t), \mathbf{u}_{\rm mpc}(t)) < \frac{\partial V}{\partial \mathbf{x}}\mathbf{f}(\mathbf{x}(t), \mathbf{u}_{\rm n}(\mathbf{x}(t))) \le 0$. Obviously, in this case, V is strictly decreasing. In the second case, the MPC scheme finds $\mathbf{u}_{\rm mpc}(t) = \mathbf{u}_{\rm n}(\mathbf{x}(t))$. Since $\mathbf{u}_{\rm n}(\mathbf{x})$ globally stabilizes (8), $\mathbf{x}(t)$ converges to zero as $t \to \infty$. We conclude that $\mathbf{u}_{\rm mpc}(t)$ globally stabilizes (8). □

The design of the proposed MPC controller is as follows. The stage cost is chosen as the quadratic form

$$l(\bar{\mathbf{x}}(\tau), \bar{s}(\tau), \bar{\mathbf{u}}(\tau)) = \mathbf{x}^{\rm T}(\tau)Q\mathbf{x}(\tau) + \mathbf{u}_{\rm a}^{\rm T}(\tau)R\mathbf{u}_{\rm a}(\tau). \quad (13)$$

In (13), $Q \in \mathbb{R}^{3\times 3}$ denotes a diagonal positive definite matrix that penalizes the path following error, whereas $R \in \mathbb{R}^{2\times 2}$ is a diagonal, positive definite weighting matrix that penalizes the inputs. This choice of the stage cost trivially satisfies *Assumption A2.1.* In what concerns the existence of a global Lyapunov function and its associated

constrained control law, it is sufficient to verify that the Lyapunov function V_{L} given by (7) and the control law for (v, r_χ) in (5) satisfy the *Assumption A2.2.*

4. SIMULATIONS

In this section, we present the results of simulations to show the efficacy of the proposed path following controllers in solving the input constrained path following problem. In the first subsection, we use the path following error system model (4) to verify the main theoretical results presented in Section 3. In the subsequent subsection, to show the robustness of the proposed controllers and their applicability in practice, we perform the simulations with a realistic model of Medusa, a prototype AMV that has been intensively used in several European research projects, see (Abreu et al. (2016)).

4.1 Simulation with a Kinematic Model

We consider the vehicle following the path parameterized by the arc length s with varying curvature $\kappa(s) = 0.1\sin(0.1s)\mathrm{m}^{-1}$. The vehicle inputs are constrained with $0 \leq U \leq 1.2\mathrm{m\,s}^{-1}$ and $|r| \leq 0.5\mathrm{rad\,s}^{-1}$. The speed profile along a path is specified as $v_{\mathrm{d}}(s) = 0.8{+}0.2\cos(0.1s)\mathrm{m\,s}^{-1}$. Thus, we obtain $\max(v_{\mathrm{d}}(s)) = 1\mathrm{m\,s}^{-1}$, $\max(\kappa(s)) = 0.1\mathrm{m}^{-1}, r_{\chi\max} = 0.5\mathrm{rad\,s}^{-1}$. We set $v_{\max} = 1.5\mathrm{m\,s}^{-1}$, thus satisfying assumptions A1.3 and A1.4. This implies feasibility of the path following problem. The tuning parameters for the nonlinear Lyapunov-based controller (5) are set to $k_1 = 0.5, k_2 = 0.175$, and $k = 0.35$. Clearly, they satisfy (6).

In the proposed MPC scheme, we construct the contractive constraint (11d) using the Lyapunov function (7) and the auxiliary stabilizing control law (5) with the above tuning parameters for the Lyapunov-based controller. The weighting matrices in the cost function (13) are chosen as Q=diag$(1, 1, 1)$ and R=diag$(1, 10)$. The sampling time is chosen as $\delta = 0.2$s and the prediction horizon is set to $T_{\mathrm{p}} = 1$s. To solve the finite optimal control problem $\mathcal{OCP}(t, \mathbf{x}(t), s(t), T_{\mathrm{p}})$, we use the open source optimization framework Casadi and the interior-point solver IPOPT (Andersson (2013)).

The path following error system is initialized at $[\mathbf{x}(0); s(0)] = [20\mathrm{m}; 10\mathrm{m}; \pi/2; 0\mathrm{m}]$. The performance of the proposed controllers is shown in Fig. 4.1. It is visible that the Lyapunov function is monotonically decreasing over time and converges to zero with both controllers. However, due to the contractive constraint, the path following error controlled by the MPC scheme has faster convergence rate. The figure also shows that the speed, the heading rate and the speed of the virtual reference satisfy the input constraints (black dash lines) with both controllers.

4.2 Simulation with a Realistic Model of the Medusa AMV

To show the applicability of the control method derived we perform simulations with a realistic model of a Medusa vehicles. The Medusa model adopted has been intensively used in simulation work as the last step before the execution of real time tests with the actual Medusa vehicles at sea (see (Abreu et al. (2016)) for the details of the vehicle). We notice that realistic Medusa model contains the kinematics model (1) coupled with two autopilots that track

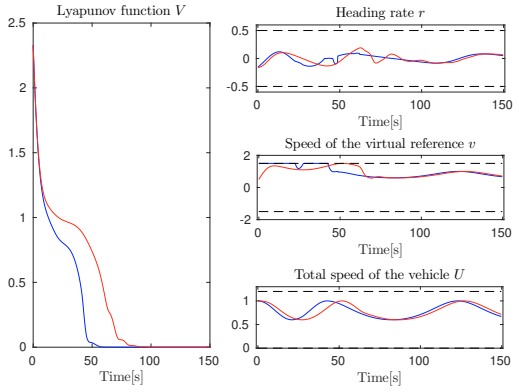

Fig. 4.1. Performance of the Lyapunov-based controller (red) and the MPC (blue) scheme for the input constrained path following problem. Black dash lines represent the bounds on the inputs.

the desired total speed and heading rate issued by a path following controller, the dynamics of the Medusa vehicle, and the dynamics of the thrusters. In the Medusa model, it is assumed that the total speed U can be measured or estimated using GPS when the vehicle is at the surface, or using a Doppler in bottom-lock mode when the vehicle is underwater.

The autopilots admit the reference commands for linear speed from 0 to $1\mathrm{m\,s}^{-1}$, and the references for heading rate from -0.3rad s^{-1} to $0.3\mathrm{rad\,s}^{-1}$. We assume that the ocean current is constant, with $v_{\mathrm{cx}} = 0.2\mathrm{m\,s}^{-1}, v_{\mathrm{cy}} = 0.2\mathrm{m\,s}^{-1}$. The current is estimated using the estimator described in (Vanni et al. (2008)). The desired speed profile is set as $v_{\mathrm{d}}(s) = 0.6 + 0.2\cos(0.1s)$. The curvature of the path is $\kappa(s) = 0.1\sin(0.1s)$.

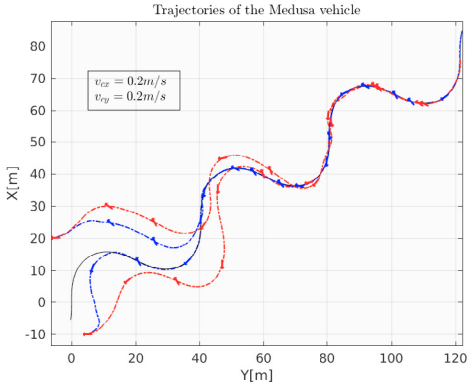

Fig. 4.2. Trajectories of the Medusa vehicle under a constant ocean current. The red-dash curves are obtained with the Lyapunov-based controller, whereas the blue-dash curves are obtained with the MPC scheme. The desired path is indicated in black.

Trajectories of the vehicle initialized with different positions and orientations are depicted in Fig.4.2 while Fig.4.3 shows the performance of the Lyapnov based and the MPC controllers. It can be observed from Fig. 4.2 that regardless of the starting positions and orientations, the vehicle always converges to the path with both proposed controllers. In Fig.4.3, it is clear that the inputs satisfy their assigned constraints (black dash lines). Similar to the

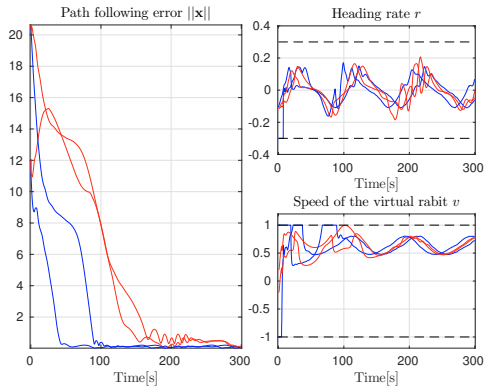

Fig. 4.3. Performances of the Lyapunov-based controller (red) and the MPC controller (blue) simulated with realistic model of the Medusa vehicle.

kinematics simulation, we observe that the MPC controller outperforms the Lyapunov-based controller with faster convergence and smaller error at steady state. Overall, the controllers show robustness against model mismatch due to the effect of the inner loops, the vehicle dynamics, and the error incurred in the current estimation.

5. CONCLUSION

In this paper, we have shown that the input-constrained path following problem for autonomous marine vehicles can be solved either with a Lyapunov-based method or with Model Predictive Control. The main contribution of this work lies in the fact that with the proposed controllers, the path following error is globally asymptotically stable, implying that the vehicle converges to and follows its assigned path, regardless of its initial position and orientation. This result is not only important from a theoretical standpoint but also makes it attractive for practical implementations. We also shown that due to a contractive constraint included in the proposed MPC, the latter speeds up the convergence of the path following error, when compared to the performance obtained with the Lyapunov-based controller.

REFERENCES

Abreu, P.C., Botelho, J., Góis, P., Pascoal, A., Ribeiro, J., Ribeiro, M., Rufino, M., Sebastião, L., and Silva, H. (2016). The MEDUSA class of autonomous marine vehicles and their role in eu projects. In *IEEE OCEANS*, 1–10.

Aguiar, A.P. and Hespanha, J.P. (2007). Trajectory-tracking and path-following of underactuated autonomous vehicles with parametric modeling uncertainty. *IEEE Transactions on Automatic Control*, 52(8), 1362–1379.

Alessandretti, A., Aguiar, A.P., and Jones, C.N. (2013). Trajectory-tracking and path-following controllers for constrained underactuated vehicles using model predictive control. In *Control Conference (ECC)*, 1371–1376.

Andersson, J. (2013). *A General-Purpose Software Framework for Dynamic Optimization*. PhD thesis, Arenberg Doctoral School, KU Leuven.

Bibuli, M., Bruzzone, G., Caccia, M., and Lapierre, L. (2009). Path-following algorithms and experiments for an unmanned surface vehicle. *Journal of Field Robotics*, 26(8), 669–688.

Caharija, W., Pettersen, K.Y., Bibuli, M., Calado, P., Zereik, E., Braga, J., Gravdahl, J.T., Sørensen, A.J., Milovanović, M., and Bruzzone, G. (2016). Integral line-of-sight guidance and control of underactuated marine vehicles: Theory, simulations, and experiments. *IEEE Transactions on Control Systems Technology*, 24(5), 1623–1642.

de la Pena, D.M. and Christofides, P.D. (2008). Lyapunov-based model predictive control of nonlinear systems subject to data losses. *IEEE Transactions on Automatic Control*, 53(9), 2076–2089.

De Luca, A., Oriolo, G., and Samson, C. (1998). Feedback control of a nonholonomic car-like robot. *Robot motion planning and control*, 171–253.

Fossen, T.I. (2011). *Handbook of marine craft hydrodynamics and motion control*. John Wiley & Sons.

Khalil, H.K. (2002). *Nonlinear systems*. Prentice Hall, New Jewsey, 3 edition.

Lapierre, L., Soetanto, D., and Pascoal, A. (2006). Nonsingular path following control of a unicycle in the presence of parametric modelling uncertainties. *International Journal of Robust and Nonlinear Control*, 16(10), 485–503.

Mayne, D.Q., Rawlings, J.B., Rao, C.V., and Scokaert, P.O. (2000). Constrained model predictive control: Stability and optimality. *Automatica*, 36(6), 789–814.

Vanni, F., Aguiar, A.P., and Pascoal, A.M. (2008). Cooperative path-following of underactuated autonomous marine vehicles with logic-based communication. *IFAC Proceedings Volumes*, 41(1), 107 – 112. 2nd IFAC Workshop on Navigation, Guidance and Control of Underwater Vehicles.

Yu, S., Li, X., Chen, H., and Allgöwer, F. (2015). Nonlinear model predictive control for path following problems. *International Journal of Robust and Nonlinear Control*, 25(8), 1168–1182.

Appendix A. DYNAMICS OF THE COURSE ANGLE

We recall that $\chi = \arctan 2(\dot{y}, \dot{x})$, thus

$$\dot{\chi} = \frac{\ddot{y}\dot{x} - \dot{y}\ddot{x}}{U^2}, \quad U = \sqrt{\dot{x}^2 + \dot{y}^2}.$$

Differentiating (1) with $v_r = 0$, we obtain

$$\ddot{x} = \dot{u}_\mathrm{r}\cos\psi - u_\mathrm{r} r \sin\psi \ , \ \ddot{y} = \dot{u}_\mathrm{r}\sin\psi + u_\mathrm{r} r\cos\psi.$$

Substituting the above in $\dot{\chi}$, we obtain

$$\dot{\chi} = -\frac{\dot{u}_\mathrm{r}}{U^2}\|\mathbf{v_c}\|\sin(\alpha-\psi) + \frac{r}{U^2}\left(u_\mathrm{r}^2 + u_\mathrm{r}\|\mathbf{v_c}\|\cos(\alpha-\psi)\right). \tag{A.1}$$

Note that $U^2 = (u_\mathrm{r}\cos\psi + v_{\mathrm{cx}})^2 + (u_\mathrm{r}\sin\psi + v_{\mathrm{cy}})^2$. Solving for the positive square-root of u_r, we obtain

$$u_\mathrm{r} = -\|\mathbf{v_c}\|\cos(\alpha-\psi) + m, \tag{A.2}$$

where $m := \sqrt{U^2 - \|\mathbf{v_c}\|^2\sin^2(\alpha-\psi)}$. Thus,

$$\dot{u}_\mathrm{r} = r\|\mathbf{v_c}\|\sin(\alpha-\psi)\left(-1 + \frac{\|\mathbf{v_c}\|\cos(\alpha-\psi)}{m}\right) + \frac{U\dot{U}}{m}. \tag{A.3}$$

Using (A.2) and (A.3), (A.1) can be simplified as

$$\dot{\chi} = r\left(1 - \frac{\|\mathbf{v_c}\|\cos(\alpha-\psi)}{m}\right) - \frac{\dot{U}\|\mathbf{v_c}\|\sin(\alpha-\psi)}{Um}.$$